Development of a Compound Energy System for Cold Region Houses using Small-Scale Natural Gas Cogeneration and a Gas Hydrate Battery

Shin'ya Obara[a*], Yoshinobu Kikuchi[b], Kyosuke Ishikawa[b], Masahito Kawai[c], and Kashiwaya Yoshiaki[d]

[a]Power Engineering Laboratory, Department of Electrical and Electronic Engineering, Kitami Institute of Technology, Koen-cho 165, Kitami, Hokkaido 090-8507, Japan

*obara@mail.kitami-it.ac.jp

phone/FAX +81-157-26-9262

[b]Power Engineering Laboratory, Graduate School of Electrical and Electronic Engineering, Kitami Institute of Technology, Koen-cho 165, Kitami, Hokkaido 090-8507, Japan

[c]Department of Mechanical Engineering, National Institute of Technology, Ichinoseki College, Takanashi Hagishyo, Ichinoseki, Iwate 021-8511, Japan.

[d]Graduate School of Energy Science, Kyoto University, Yoshidahonmachi, Kyoto Sakyo-ku, Kyoto 606-8501, Japan

Abstract

In this study, an independent energy system for houses in cold regions was developed using a small-scale natural gas CGS (cogeneration), air–source heat pump, heat storage tank, and gas hydrate battery (GHB). Heat sources for the GHB were the ambient air and geothermal resources of the cold region. The heat cycle of CO_2 hydrate as a source of energy was also experimentally investigated. To increase the formation speed of CO_2 hydrates, a ferrous oxide–graphite system catalyst was used. The ambient air of cold regions was used as a heat source for the formation process (electric charge) of the GHB, and the heat supplied by a geothermal heat exchanger was used for the dissociation process (electric discharge). Using a geothermal heat source, fuel

consumption was halved because of an increased capacity for hydrate formation in the GHB, a shortening of the charging and discharging cycle, and a decrease in the freeze rate of hydrate formation space. Furthermore, when the GHB was introduced into a cold region house, the application rate of renewable energy were 47% - 71% in winter. The spread of the GHB can greatly reduce fossil fuel consumption and the associated greenhouse gases released from houses in cold regions.

Keywords: CO_2 hydrate, Cogeneration, Compound Energy System, Small Temperature Difference Power Generation

1. Introduction

Various gases can form gas hydrates, in which gas molecules are trapped inside "cages" of hydrogen-bonded water molecules. Many industrial applications of the hydrates have been investigated, particularly of methane and carbon dioxide hydrates. With regard to methane hydrates, considerable research has focused on the highly efficient extractive technology of gas hydrate [1-3] and economical use of methane [4-7]. On the other hand, the methane hydrates also attracts attention as a technologically highly efficient means for transporting natural gas. Study of natural-gas transportation is investigated by Javanmardi J et al. [8], Hu Get al. [9], and Kim N J et al. [10]. Studies have further investigated the use of gas hydrates for the storage of cold energy by Xie Y et al. [11], Bi Y et al. [12], Daitoku T and Utaka Y [13], and capture of CO_2 by Aspelund A et al. [14, 15]. A prominent characteristic of gas hydrates is that the phase equilibrium condition of formation and dissociation occurs under large pressure differences with relatively small temperature changes. For example, on the phase equilibrium curve of formation and dissociation for CO_2 hydrate, a temperature change from 0 ℃ to 10 ℃ exhibits a corresponding pressure difference of about 3 MPa [16]. Therefore, when the pressure change caused by the dissociation expansion gas of a hydrate is released to an actuator, large amounts of power can be generated by a relatively small change in temperature. Furthermore, since gas hydrates can be easily stored, the combination of gas hydrates and an actuator can serve as an electric charge-and-discharge apparatus (gas hydrate battery: GHB). The large heat to power ratio

make this an important energy source for cold regions during winter where low cost and clean energy is essential. Therefore, the use of geothermal heat pumps, employing electric storage heaters for surplus power at midnight and early in the morning has become more common [17-19]. However, the technology described above requires electric power, and if fossil fuels are to be avoided, it means an increase in either thermal or nuclear power generation. The purpose of this study was, therefore, the development of a complex of cogeneration and the GHB system, using a small-scale natural gas engine [20, 21] to reduce fossil fuel consumption for cold regions during winter, and subsequently greenhouse gases.

For this purpose, we use a carbon dioxide-based GHB, where the heat change was produced from low temperature of the ambient winter air in the cold region and high temperature of the heat medium, warmed by a geothermal heat exchanger. Power consumption is very small as the GHB is operated only by the circulating pump for the heat media. However, the capacity of gas hydrate generator and gas hydrate accumulator is large and requires repeated charge and discharge at regular intervals, as is common with all batteries. Therefore, in this paper we clarify the following: (1) the configuration and capacity of a small-scale natural gas CGS (cogeneration) and the GHB energy system for houses in cold regions; (2) the operation method for each piece of equipment constituting the system; and (3) the relation between heat to power ratio and fuel consumption of the proposed system. When these points are understood, the distributed energy can be improved drastically for cold regions, minimizing the accompanying winter heat demand and consumption of fossil fuels.

2. System Configuration

2.1 System Scheme

Figure 1 shows the conventional and proposed distributed energy systems for houses in cold regions investigated in this paper. A conventional CGS for individual houses consists of the air heat-source heat pump, heat storage tank and heat supply by a natural-gas engine generator (Fig. 1a). The fuel consumption in System A (Fig. 1b) and the CGS in System B (Fig. 1c) is compared with the conventional CGS system (Fig. 1a). Heat on the demand side (space heating and hot water supply) in System A is supplied by the CGS exhaust heat and air heat-source heat pump, while heat for the

dissociation process (electric discharge) of the GHB is supplied by an approximately 10–15 ℃ heat medium warmed by a geothermal heat exchanger. Moreover, for the formation processes (electric charge) of gas hydrates, ambient air, absorbed by a radiator, is used as a source of cold energy (yellow arrows in Figs. 1b and 1c). Alternatively, on the demand side in System B, heat is supplied by the CGS exhaust heat, air heat source heat pump, and partially supplied by the geothermal heat exchanger. An auxiliary boiler is operated when high temperature water supply is required in System A and System B; however, it is not further discussed in this paper. Moreover, the capacity of the geothermal heat exchanger is large in System B because geothermal heat provides part of the heat supply to the demand side (space heating and hot water supply), increasing the equipment cost of System B relative to System A. However, due to the large decrease in power consumption of the air heat source heat pump in System B, fuel consumption of the entire CGS system is expected drastically decrease.

2.2 Energy Flow and Energy Balance Equation

The energy flow and energy balance of each system are described below by Figs. 1a–c. Green, red, blue, and yellow arrows in Fig. 1 are natural gas fuel, electricity, heat, and the formation process of gas hydrates, respectively. The symbols q_f, p, and h in Fig. 1 refer to fuel flow rate, electricity, and heat based on the calorific value, respectively, while η, T, and COP refer to efficiency, temperature, and the performance coefficient of the heat pump. The subscript t is sampling time, θ_{cgs} is the heat to power ratio of the CGS output, and H_{st} is the heat storage quantity.

2.2.1 Conventional System (Fig. 1 a)

Electricity output is obtained from the CGS alone and is supplied to the demand side and air heat source heat pump (Eq. (1)). The heat output from the CGS is calculated using Eq. (2), with heat storage ($H_{st,t}$) obtained from Eq. (3) using heat storage start and finish times, hss and hse, respectively. The heat released from the heat storage tank is calculated using Eq. (4), which introduces the efficiency of thermal storage ($\eta_{hst,t}$) into each sampling time from the start (ohs) to finish (ohe) of heat output. The thermal power ($h_{ahp,t}$) of the air heat source heat pump is obtained from

$COP_{ahp,t} \cdot p_{ahp,t}$ by giving the electricity ($p_{ahp,t}$) to the heat pump (Eq. (5)). The heat demand ($h_{demand,t}$) is the sum of the thermal power of the heat storage tank and heat pump, as shown in Eq. (6).

$$\frac{1}{\theta_{cgs,t}+1} \cdot q_{f,t} = p_{cgs,t} = p_{demand,t} + p_{ahp,t} \tag{1}$$

$$h_{cgs,t} = \frac{\theta_{cgs,t}}{\theta_{cgs,t}+1} \cdot q_{f,t} \tag{2}$$

$$H_{st,t} = \sum_{t=hss}^{hse} h_{cgs,t} \tag{3}$$

$$h_{hst,t} = \sum_{t=ohs}^{ohe} \left(\eta_{hst,t} \cdot h_{st,t} \right) \tag{4}$$

$$h_{ahp,t} = COP_{ahp,t} \cdot p_{ahp,t} = h_{amb,t} + p_{ahp,t} \tag{5}$$

$$h_{demand,t} = h_{hst,t} + h_{ahp,t} \,. \tag{6}$$

2.2.2 System A (Fig. 1 b)

Since electricity of System A is output from the CGS ($p_{cgs,t}$) and GHB ($p_{ghb,t}$), the balance equation of electricity is shown by Eq. (7). Furthermore, as the amount of GHB electric discharge is dependent on the dissociation temperature of the gas hydrate, as displayed in Figs. 2 and 3, the function $\psi(T_{ghb})$ of dissociation temperature is introduced. The GHB electric discharge is calculated by Eq. (8) using the heat ($h_{gth,ghb,t}$) of the heat medium supplied to the GHB via the geothermal heat exchanger. Although the heat medium is circulated with a pump between the geothermal heat exchanger and the GHB, the power consumption ($\Delta p_{pump,t}$) in the circulation pump is calculated by Eq. (9), where ρ_w, $Q_{w,t}$, η_{pump}, and H represent density of the heat medium, volumetric flow, pump efficiency, and total head of actual pump head and loss head, respectively. Although thermal power of the CGS is the

same as previously described in Eq. (2), the exhaust heat ($h_{cgs,t}$) of the CGS and the thermal power ($h_{ahp,t}$) of air heat source heat pump (Eq. (5)) are stored in a heat storage tank ($H_{st,t}$), as shown in Eq. (10). Moreover, the thermal power from the heat storage tank supplied to the demand side ($h_{demand,t}$) is calculated by Eq. (11). The heat ($h_{hst,ghb,t}$) to the GHB is supplied by controlling the flow of the heat medium by the geothermal heat exchanger. In Figs. 1b and 1c, the energy flow (yellow arrows) is provided for the charging operation of the GHB in which gas hydrates are formed. Cold energy ($h_{ahb,amb,t}$), required for the generation process of gas hydrates, is absorbed from the ambient air using a radiator.

$$\frac{1}{\theta_{cgs,t}+1}\cdot q_{f,t} = p_{cgs,t} + p_{ghb,t} = p_{demand,t} + p_{ahp,t} + \Delta p_{pump,t} \tag{7}$$

$$p_{ghb,t} = \psi\left(T_{ghb}\right)\cdot h_{gth,ghb,t} \tag{8}$$

$$\Delta p_{pump,t} = \frac{\rho_w \cdot g \cdot Q_{w,t} \cdot H}{\eta_{pump}} \tag{9}$$

$$H_{st,t} = \sum_{t=hss}^{hse}\left(h_{cgs,t} + h_{ahp,t}\right) \tag{10}$$

$$h_{demand,t} = \sum_{t=ohs}^{ohe}\left(\eta_{hst,t}\cdot h_{st,t}\right) \quad \text{System B 同じ.} \tag{11}$$

2.2.3 System B (Fig. 1c)

In addition to the heat balance of System A, geothermal heat is introduced into some heat loads in System B. Therefore, in addition to the power consumption ($\Delta p_{pump,t}$) of the heat-medium circulating pump for gas hydrate dissociation, the consumption ($\Delta p_{pump,h,t}$) of the heat demand pump is applied to the electricity balance equation (Eq. (12)). The CGS exhaust heat ($h_{cgs,t}$), thermal power ($h_{ahp,t}$) of the air heat source heat pump, and heat from the geothermal heat exchanger ($h_{gth,hst,t}$) are all stored

in a heat storage tank in System B, as shown in Eq. (13). The thermal power of the air heat source heat pump (Eq. (5)), the amount of electric discharge in the GHB (Eq. (8)), the power consumption in the pump (Eq. (9)), and the thermal power from a heat storage tank (Eq. (11)) are all as described by System A equations given in Section 2.2.2.

$$\frac{1}{\theta_{cgs,t}+1}\cdot q_{f,t} = p_{cgs,t} + p_{ghb,t} = p_{demand,t} + p_{ahp,t} + \Delta p_{pump,t} + \Delta p_{pump,h,t} \tag{12}$$

$$H_{st,t} = \sum_{t=hss}^{hse}\left(h_{cgs,t} + h_{ahp,t} + h_{gth,hst,t}\right). \tag{13}$$

3. Gas hydrate Battery (GHB)

3.1 Phase Diagram and Characteristics of Gas Hydrates

Figure 2 is a phase diagram of gas hydrates formed by various types of gases [22]. In this paper, a carbon dioxide hydrate was selected based on the temperature, pressure, and safety conditions of the experiment. CO_2 hydrates have a large latent heat of formation and dissociation; furthermore, with the temperature gradient of ambient air in cold regions of Japan and the low temperature exhaust heat, a large differential pressure can be obtained from the phase equilibrium of formation and dissociation. As observed in Fig. 2, when temperature of CO_2 hydrate changes from 0 ℃ to 10 ℃, pressure changes by approximately 3 MPa. Using this phase change of CO_2 hydrates, we developed a small temperature gradient heat cycle based on the characteristic weather of a cold district.

Figure 3 is a CO_2 hydrate phase diagram, describing operating points (points A–C) within a proposed system operation. In this system, an airtight container is filled with CO_2 and water, with the initial state in the container represented by Point A in Fig. 3. When the airtight container is cooled, the resulting state, indicated by Point B (Fig. 3), is on the freezing point of water because the water in the container starts to freeze. When the airtight container is further cooled, the state in the container will move toward Point C (Fig. 3), where the formation rate of CO_2 hydrate will be considerably slowed as the water becomes ice. Therefore, it is necessary to control the temperature of the system to avoid complete freezing of the water in the airtight container. The ambient air of a cold region is used for

the low temperature heat source from Point A to Point C in Fig. 3 in the proposed system. However, as the ambient temperature may be less than −20 ℃, freezing of the water in the airtight container must be prevented by stopping the uptake of the ambient air or supplying heat of a slightly higher temperature from an additional heat source. The exhaust heat of the CGS and a heat pump can be used as heat sources to move the proposed system from Point C to Point A, eliminating the requirement of a backup boiler in the system. Therefore, in this paper, geothermal heat is used as a high temperature heat source moving the system from Point C to Point A (Fig. 3). In the GHB, an actuator is driven by the differential pressure created by moving from Point A to Point C. Electricity can then be extracted by connecting a generator to the actuator. As gas hydrates can be stored, the storage energy of the GHB can be shifted in time and discharged as electricity similar to a common battery.

3.2 Formation and Dissociation Experiment of CO_2 Hydrates

Figure 4 shows the basic experimental system created to investigate the dissociation and formation characteristics of CO_2 hydrate. The test equipment supplies the heat medium for cooling and heating the inner pipe of the double tube heat exchanger, as shown in Fig. 4a, and the space between outer pipes is filled with pure water and CO_2 (described hereafter as the test space). The capacity of this test space is approximately 100 cm^3, and the length of pipe for the examination space is about 370 mm. The outer and inner diameters of the outside pipe are 25.4 mm and 21.2 mm, respectively, and those for the inner pipe are 12.8 mm and 10.2 mm, respectively. The heat medium is supplied to the inner pipe of the double tube heat exchanger, to heat and cool the fluid in the test space, which leads to the formation and dissociation of CO_2 hydrate in the test space. CO_2 for gas hydrates and N_2 for inert gas replacement can be supplied to the experimental device, as shown in Fig. 4b. Temperature sensors (T-type thermocouple) are installed in the outer wall of the outside pipe and the entrance of the heat medium, and the pressure in the test space is measured using a pressure sensor.

3.3 Optimization of the Formation Rate of CO_2 Hydrates

The formation rate of CO_2 hydrates under the best conditions is approximately 5×10^{-3} wt%/s; therefore, it requires approximately 17 min to form 5 wt% of CO_2 hydrates [23]. However, to form gas

hydrates with high efficiency, vigorous stirring of the mixing fluid of CO_2 and water is necessary. Since the formation rate of gas hydrate decreases dramatically in the absence of stirring, the capacity of a gas hydrate tank becomes very large. To avoid equipment complication (installation of a stirrer into the high pressure airtight container) and to decrease power consumption of the stirrer, a catalyst that improves the formation rate of methane hydrate [24] was used in this study. Referring to the study of Takahata et al. [24], to prepare the powdered catalyst, ferrous oxide is sintered in an electric furnace (1000 ℃) for 24 h, and 50.0 g of the ferrous oxide and 14.3 g of graphite were milled at a mixture ratio of O/C = 1.0 for 48 h (Fig. 5). The catalyst was introduced into the test space, as shown in Fig. 4a, at a concentration of 0.5 wt%.

3.4 Configuration of the Gas hydrate Battery (GHB)

Figure 6 shows the configuration of the GHB and the fluid flow. More specifically, Fig. 6a represents the formation process of CO_2 hydrate (in other words, electric charge), and Fig. 6b depicts the gas dissociation process (electric discharge). The GHB consists of two sets of plate-type heat exchangers (gas hydrate generator, gas hydrate accumulator), and one actuator and generator set. The heat exchanger at the bottom of Figs. 6a and 6b is a gas hydrate generator, and the upper part is a gas hydrate accumulator. The water and CO_2 mixing fluid is sealed by the high pressure of the hydrate formation space between the plates of the gas hydrate generator. The hydrate formation space described above is equivalent to the test space of the double-tube-type heat exchanger used in the basic experiment, represented in Fig. 4a. To heat and cool the water and CO_2 mixing fluid for forming CO_2 hydrate, the heat medium (antifreezing solution) is introduced into the space between the plates.

As shown in Fig. 6a, when cold energy is supplied to the gas hydrate generator, the water and CO_2 mixing fluid is cooled, and gas hydrate is, therefore, formed according to the phase diagram of Fig. 3. When the warm heat medium, provided by high temperature heat sources, is supplied to the gas hydrate accumulator, CO_2 smoothly returns to the gas hydrate generator because of the expansion of CO_2 in the heat exchanger. However, when the fluid flows change from Fig. 6a to 6b and heat medium is supplied to the gas hydrate generator, the CO_2 hydrate formed in the hydrate formation space is heated, and dissociation of CO_2 commences. The resultant high-pressure dissociated gas, supplied to

the actuator, generates electricity, and the CO_2 gas exiting the actuator is stored in the gas hydrate accumulator. The pressure of the gas hydrate and that of the gas hydrate accumulator balances, dissociation of gas is completed, and the actuator stops. The fluid flows are changed again from Fig. 6b to 6a, and the system returns to the formation of gas hydrates.

4. Compound Energy System for Cold Region Residences

Figure 7 is a configuration of the small-scale engine cogeneration and a GHB energy system for houses in the cold region investigated in this paper. The solid lines and broken lines indicate dissociation and formation processes, respectively, and the control line is represented by a black broken line. The introduction of the heat-exchange system (red solid line), which connects a buffer tank and thermal storage tank (Fig. 7), into System B is described in Section 2.1. As the heat to power ratio in a cold region is large, the rated capacity of the generator is dependent on the magnitude of heat load that exceeds the CGS exhaust heat. To control the rated capacity of the generator for System A and System B, an air heat source heat pump is introduced. In the analysis, the coefficient of performance (COP) of the air heat source heat pump, referred to present Japanese products, was set to 2.0 and 4.5 corresponding to a heat-source temperature of −20 ℃ to 20 ℃ [25]. However, even with the additional heat pump, the capacity of the engine generator is larger in cold regions where the winter heat to power ratio exceeds 10. Therefore, in addition to the air heat source heat pump in System B, heat for space heating (red line in Fig. 7) is also required from a heat medium (about 10 ℃ to 15 ℃) warmed by a geothermal heat exchanger. Because of the need to supply this heat load for space heating and to heat the water to 10–15 ℃ using geothermal heat from ambient air, rated capacity of System B engine generator becomes smaller than that of System A. Moreover, since installation of the geothermal heat exchanger is expensive, the capacity (quantity of heat collecting) of the geothermal heat exchanger is determined to be 30% of the rated output of a heat pump in the following section.

5. Analysis Method

5.1 Analysis Conditions

5.1.1 Ambient Air Temperature

The ambient air temperature data in Kitami from November 2012 to March, 2013, as shown in Fig. 8, was used as an introductory case for the proposed system. Because the air temperature data (which constitutes the average values for all sampling periods) from April to November (i.e., spring, summer, and autumn) does not reach the freezing point, the formation of CO_2 hydrate is difficult. Therefore, operation of the GHB in Kitami is limited to a period from December to March (winter season).

5.1.2 Energy Demand

Figs. 9a and 9b show the assumed power and heat loads of a single-family house used in this analysis. The load patterns of Fig. 9 were prepared based on a study by Narita [26], considering the energy demand of Kitami. Because the cooling and heating load is contained in the heat demand, the monthly power load varies slightly. The average heat to power ratio of a February day using Fig. 9 is 15.9. Although electricity for the varying power load (Fig. 9a) can be supplied by the proposed system, electricity production using our CGS system (System A and System B) is constant. For the time when electricity exceeds the power load, shown in blue in Fig. 9a, of the CGS changes surplus power into heat using the heat pump. The space heating method employed in this paper is operational for 24 h and assumes a super insulated airtight house, as is the current building practice. The heat is always supplied to the demand side of the system through a heat storage tank. The heat supply on any representative day is, therefore, the same as the sum total of the heat load for every month, as shown in Fig. 9b. Although the heat generation of the system for every sampling time ($h_{cgs,t} + h_{ahp,t}$ in System A, $h_{cgs,t} + h_{ahp,t} + h_{gth,hst,t}$ in System B) is not constant, heat can be supplied to the demand side by preparing the heat storage tank. Moreover, as previously mentioned, fuel consumption by the backup boiler for the hot water supply of each system is not included in this paper.

5.2 Analysis Flow

Figure 10 depicts the analysis flow of System A and System B, with each block represented by a letter from (a) to (o). Various types of initial data used for the analysis are input in Block (a). The main input data is the temperature–pressure characteristics of gas hydrates (Fig. 3), ambient air

temperature (Fig. 8), load pattern of electricity and heat (Fig. 9), heat to power ratio of the CGS (2.0), COP table of the heat pump [25], temperature of geothermal heat exchange (15 ℃), efficiency of pumps (0.75), freeze rate of hydrate formation space (90%), and heat storage loss (10%). Operation of the system is analyzed by changing the hydrate formation space (loop of Blocks (b)–(o)) and the rated output of the CGS (Block (c)). The repetition pattern of electric charge and electric discharge of the GHB has been input into Block (d) earlier, with the electric charge (formation gas hydrate) and electric discharge (dissociation of gas hydrate) repeated every 6 h. Repetition of Blocks (e)–(l) is the loop formation of the sampling time for a representative day, the power balance and heat balance, as described in Sections 2.2.2 and 2.2.3, which are calculated in Blocks (f) to (k). The fuel consumption of the CGS is calculated from Eq. (7) or (12) in Block (m). As the natural-gas engine generator of the CGS is operated by a fixed load, the power generation efficiency for these calculations is constant at 26.3% [27]. To determine the rated output of the CGS at the time of minimum fuel consumption, after returning to Block (c) by the conditional branch of Block (n) and controlling the rated CGS output, the loop formation of Block (e)–(l) is re-calculated. The capacity of hydrate formation space, rated output of the CGS, fuel consumption, and operation method for each piece of equipment (amount of power) can be determined by the analysis flow (Fig. 10). The interval of sampling time is 1 hour and all variables are discontinuous. Common personal computer and MS-Excel are used for analysis.

6. Analysis Results and Consideration

6.1 Results of Basic Experiment, and Determination of Specifications of the GHB Heat Exchanger

Figure 11 shows the results of formation and dissociation experiment using the basic CO_2 hydrate system described in Section 3.2 (Fig. 4). Figure 11 (a) shows an experimental result for the formation and dissociation processes of CO_2 hydrate using a heat medium of −5 ℃ and 30 ℃, respectively. The dissolution of CO_2 is thought to strongly influence the formation and dissociation process of gas hydrate. As the solubility of CO_2 is large, it is necessary to ensure CO_2 is fully dissolved in water prior to the gas hydrate formation and dissociation experiment. As such, the first hour is dedicated as a preparation period for dissolving CO_2 (Fig. 11). All the experiments are started after the amount of dissolutions of CO_2 is saturated mostly.

Figure 11b shows the experimental results after the addition of the catalyst to improve the CO_2 hydrate formation rate described in Section 3.3. The formation rate of the hydrates is clearly increased taking approximately 30 min (between 1.0 and 1.5 h, Fig 11b) relative to the 2 h formation time (between 1.0 h and 3.0 h, Fig 11a) of the conventional method. Using the GHB of the proposed system, it becomes possible to repeat the formation (electric charge) and dissociation (electric discharge) of the gas hydrate every few hours, as shown in Fig. 11b. In this paper, the heat transfer characteristics of the plate heat exchangers, shown in Fig. 6, were designed to incorporate the more rapid formation and dissociation characteristics of the CO_2 hydrate, presented in Fig. 11b, into the GHB. The flow of the heat medium, volume of the space between plates, and heat transfer area were calibrated to increase the heat transfer between the hydrate formation space in plate heat exchangers (see Fig. 6) and the heat medium. The increased heat transfer should exceed the heat transfer of the mixing fluid and heat medium using water and CO_2 in the test space of the basic experimental system (Fig. 4a). By introducing the flow of the heat medium into Eq. (9), the power consumption of the heat-medium circulating pump was calculated. Because the Grashof number is obtained from the heat transfer area and hydrate formation space, the detailed specifications for the GHB heat exchanger can be subsequently determined from these values.

6.2 Operation of System

6.2.1 Analysis Results of Power Balances

Figures 12–14 show the operational analysis of electricity balance and heat balance for a representative day in November and February for the conventional system (Fig. 12), System A (Fig. 13), and System B (Fig. 14) with hydrate formation space of 1 m^3. The analysis was performed according to Fig. 10. The power output of the CGS shown in the operation results at the top of each figure represents as the rated power when there is the smallest output power (the least fuel consumption) in each system.

The GHB output of System A (Fig. 13) and System B (Fig. 14) have repeated charge and discharge (formation and dissociation of CO_2 hydrates, respectively) at 6 h intervals, as seen in the February results (Fig. 13b and Fig. 14b). This reason is for requiring about 6 hours, although 1 cycle of

generation and dissociation of the gas-hydrate of suitable capacity is obtained. When the interval period described above is shortened further, the capacity of hydrate formation space decreases; as a result, a miniaturization of the gas hydrate generator and accumulator is possible. On the other hand, for a representative day of November, because the air temperature is high, the GHB of System A and System B do not operate and are not seen in Figs. 13a and 14a. The operation of the GHB system is, therefore, limited to winter seasons with low ambient air temperatures.

The power consumption of the pump during the dissociation of gas hydrates is about 60% of the GHB production of electricity (Figs. 13b and 14b). The large power consumption in the heat-medium circulating pump is due to the freeze rate of hydrate formation space being set at 90%, as described in Section 5.2. A greater amount of heat is required for icy dissolution than that for the dissociation of CO_2 hydrates. Therefore, when the ambient air temperature decreases, under the formation process of gas hydrate, it is essential to avoid freezing the water in the gas hydrate generator. This is regulated by controlling the amount of ambient air uptake to the gas hydrate generator and further controlling the water temperature in the gas hydrate generator by geothermal heat. By reducing freeze rate in the hydrate formation space, the pump power consumption for dissociation of gas hydrate is drastically diminished.

6.2.2 Analysis Results of Heat Balance

With regard to heat balance, the output of total thermal power (red line of each figure) from each system fluctuated over the sampling time (bottom graph of Figs. 12–14). The reason the total thermal power output varied is because surplus power, which is calculated at each sampling time to satisfy the power balance of Eqs. (1), (7), and (12), is supplied to the heat pump and converted into heat. Therefore, the supply-and-demand difference of electricity affects heat supply. Fluctuations of the output of total thermal power are adjusted with the heat storage tank.

Because 24 h space heating in an airtight thermally insulated house is assumed, large fluctuations of the heat load (bottom figure of Figs. 12–14) and the amount of thermal power of each system do not have to be synchronized. The output of total thermal power of the conventional system (Fig. 12) and System A (13) is the sum total of the CGS exhaust heat and heat pump output. On the other hand, the

total thermal power output of System B (Fig. 14) combines the heat of the heat medium with the CGS exhaust heat and the output of the heat pump.

Moreover, as shown in Figs. 13 and 14, the heat of the geothermal heat exchanger for dissociation of the gas hydrate in System A and System B has exceeded the output of the exhaust heat of the CGS and heat pump, and the heat of the geothermal heat exchanger is large relative to the thermal power of the system. Therefore, a reduction in the use of the geothermal heat by decreasing the freeze rate of hydrate formation space, as described in Section 6.2.1, contributes to a great reduction in the equipment cost.

6.3 Fuel Consumption Characteristics

The analysis of the CGS fuel consumption in the conventional system, System A, and System B for a representative day are shown in Fig. 15a. The hydrate formation space of the GHB forms part of the analysis for System A and System B. The rate of the fuel consumption of System A and System B is presented in Fig. 15b as a percentage of the November fuel consumption of the conventional system. Since in November, the ambient air temperature is comparatively high, the GHB in System A is not operational and the fuel consumption is no different from the conventional system. In System A (Fig. 15) the fuel reduction is based solely on the introduction of the GHB. Reduction of the fuel consumption by System B, on the other hand, is due to both the GHB and geothermal heat, the latter corresponding to 30% of the thermal power of the heat pump.

The winter fuel consumption using System B can be reduced to below half that of the conventional system, by increasing the volume of the hydrate formation space. Furthermore, increasing the charging and discharging cycle of the GHB and reducing the freeze rate of hydrate formation space for System B will further reduce fuel consumption considerably for the winter season in cold regions.

6.4 Utilization Rate of Renewable Energy

Figure 16 shows the analysis of energy sources supplied to each system. The energy sources of the conventional system, electricity, heat by a natural gas CGS (Fig. 16a), and atmospheric air absorbed by an evaporator of the air heat source heat pump, is approximately 40% renewable energy during

winter (heating value of the yellow areas of Fig. 16 (a)). The percentage of the renewable energy (atmospheric air and geothermal resources) for System A (Fig. 16b) will be 30–47% from December to March and 47–71% for System B (Fig 16c). Therefore, System B, when realized, will drastically reduce fossil fuel consumption of houses in cold regions and will significantly contribute to global warming countermeasures.

6.5 Characteristics of Fuel Consumption by Heat to Power Ratio

The relation between heat to power ratio and fuel consumption obtained from the analytical calculation of each system is displayed in Fig. 17. When the hydrate formation space is large, even if the heat to power ratio increases, the fuel consumption in the CGS will be controlled.

Although power consumption by the heat pump will increase when the heat to power ratio increases, because electricity production by the GHB increases by raising the capacity of the hydrate formation space, the rate of renewable energy increases in the power supply to the heat pump. As a result, when the larger hydrate formation space of 4 m^3 and 2.8 m^3 is installed in System A and System B, respectively, the fuel consumption of the CGS becomes uniform regardless of the heat to power ratio. Although 30% of the heat load is supplied from geothermal resources in System B because the power consumption of the pump for geothermal recovery is small, output of the thermal power increases. As a result, even if the heat to power ratio of System B increases, the fuel consumption of the CGS is better controlled than that of System A.

7. Conclusions

Fundamental characteristics of compound energy systems were investigated for houses in Kitami, a cold region of Japan, which used a natural-gas CGS and the GHB associated with a small-scale engine. Our analysis compared the conventional system composed of a small-scale CGS with air heat source heat pump, and two proposed systems (System A and System B) with the GHB using the heat of ambient air and geothermal resources. System B also used geothermal resources as a partial heat supply to the demand side of the system. As a result, the following conclusions were obtained.

(1) The GHB in November is not charged (formation process of gas hydrate) due to the elevated air temperature. The effective operating period in Kitami was from December to March (winter).

(2) The conventional fuel consumption of the Kitami winter can be more than halved by increasing the volume of the hydrate formation space in System B. Furthermore, in System B, when the charging and discharging cycle of the GHB are shortened and the freeze rate of hydrate formation space is reduced, winter fuel consumption in the cold region can be further reduced. It is expected that reduction of the freeze rate of hydrate formation space is achieved by the control of the ambient air uptake quantity in the gas hydrate formation process and by further temperature control via regulated supply of the ambient air and by a geothermal resource.

(3) To improve the formation speed of the CO_2 hydrate, a ferrous-oxide–graphite system catalyst was used. The catalyst shortens the generating time of the hydrate from 3 h, with the conventional method, to 30 min. This allows the formation and dissociation (electric charge and discharge of the GHB) of the CO_2 hydrate to be repeated every several hours.

(4) The percentage of the renewable energy (air) in the conventional system was approximately 40% compared with 30–47% in System A and 47–71% in System B during winter (from December to March).

(5) When the large capacity hydrate formation space is installed in System A and System B, the fuel consumption of the CGS became uniform regardless of the heat to power ratio. This is a product of operating the heat pump by electricity with high rate of renewable energy when the heat to power ratio is large. Furthermore, although a part of the heat demand is supplied by the geothermal resource in System B, because the power consumption of the pump for geothermal recovery is small, increase in the thermal power output can be generated by relatively less power consumption.

Therefore, System B can contribute to drastic reductions in fossil fuel and a significantly contribute to global warming countermeasures for houses in cold regions.

Nomenclature

COP : Coefficient of performance

g : Acceleration due to gravity [m/s^2]

H : Total pump head [m]

H_{st} : Heat storage amount [kWh]

h : Heat [kW]

hse : Stop time of heat storage [h]

hss : Start time of heat storage [h]

ohe : Stop time of heat output [h]

ohs : Start time of heat output [h]

p : Electricity [kW]

Δp : Electricity consumption [kW]

$\Delta p_{pump,h}$: Power consumption of heat-medium circulating pump [kW]

Q : Volumetric flow [m^3/s]

q : Quantity of heat [kW]

q_f : Calorific value of fuel [kW]

T : Temperature [℃]

Greek characters

η : Efficiency [%]

η_{hst} : Efficiency of heat storage [%]

θ_{cgs} : Heat to power ratio of cogeneration output

ρ : Density

ψ : Function depending on dissociation temperature

Subscripts

ahp : Air-source heat pump

amb : Ambient

cgs : Cogeneration

ghb : Gas hydrate battery

gth : Geothermal heat

t : Sampling time [h]

w : Water

References

[1] Lang X, Fan S, Wang Y, Intensification of methane and hydrogen storage in clathrate hydrate and future prospect, Journal of Natural Gas Chemistry, 2010, 19(3): 203-209.

[2] Gabitto J, Tsouris C, Dissolution mechanisms of CO_2 hydrate droplets in deep seawaters, Energy Conversion and Management, 2006, 47(5): 494-508.

[3] Crutchley G J, Klaeschen D, Planert L, Bialas J, Berndt C, Papenberg C, Hensen C, Hornbach M J, Krastel S, Brueckmann W. The impact of fluid advection on gas hydrate stability: Investigations at sites of methane seepage offshore Costa Rica. Earth and Planetary Science Letters 2014;401:95-109.

[4] Nakoryakov E V, Misyura Y S, The features of self-preservation for hydrate systems with methane, Chemical Engineering Science, 2013, 104: 1-9.

[5] Demirbas A, Methane hydrates as potential energy resource: Part 1—Importance, resource and recovery facilities, Energy Conversion and Management, 2010, 51: 1547-1561.

[6] Wang Y, Li X, Li G, Zhang Y, Feng J, Experimental investigation into scaling models of methane hydrate reservoir, Appl. Energy, 2014, 115: 47-56.

[7] Li X, Yang B, Zhang Y, Li G, Duan L, Wang Y, Chen Z, Huang N, Wu H, Experimental investigation into gas production from methane hydrate in sediment by depressurization in a novel pilot-scale hydrate simulator, Applied Energy, 2012, 93: 722-732.

[8] Javanmardi J, Nasrifar kh, Najibi S H,Moshfeghian M, Economic evaluation of natural gas hydrate as an alternative for natural gas transportation. Applied Thermal Engineering 2005;25:1708-1723.

[9] Hu G, Ye Y, Liu C, Meng Q, Zhang J, Diao S, Direct measurement of formation and dissociation rate and storage capacity of dry water methane hydrates, Fuel Processing Technology, 2011, 92(8): 1617-1622.

[10] Kim N J, Hwan L J, Cho Y S, Chun W, Formation enhancement of methane hydrate for natural gas transport and storage, Energy, 2010, 35(6): 2717-2722.

[11] Xie Y, Li G, Liu N, Liu N, Qi Y, Liang D, Guo K, Fan S, Experimental study on a small scale of gas hydrate cold storage apparatus, Applied Energy, 2010, 87(11): 3340-3346.

[12] Bi Y, Guo T, Zhang L, Chen L, Sun F, Entropy generation minimization for charging and discharging processes in a gas hydrate cool storage system, Applied Energy, 2010, 87(4): 1149-1157.

[13] Daitoku T, Utaka Y, Separation characteristics of clathrate hydrates from a cooling plate for efficient cold energy storage, Applied Energy, 2010, 87(8): 2682-2689.

[14] Aspelund A, Gundersen T, A liquefied energy chain for transport and utilization of natural gas for power production with CO_2 capture and storage—Part 4: Sensitivity analysis of transport pressures and benchmarking with conventional technology for gas transport, Applied Energy, 2008, 86(6): 815-825.

[15] Aspelund A, Gundersen T, A liquefied energy chain for transport and utilization of natural gas for power production with CO_2 capture and storage—Part 1, Applied Energy, 2009, 86(6): 781-792.

[16] Sloan ED, Koh CA. Clathrate hydrates of natural gases. 3rd ed. New York: CRC Press; 2007.

[17] Ali M, Jokisalo J, Siren K, Lehtonen M, Combining the Demand Response of direct electric space heating and partial thermal storage using LP optimization, Electric Power Systems Research, 2014, 106: 160-167.

[18] Parameshwaran R, Kalaiselvam S, Harikrishnan S, Elayaperumal A, Sustainable thermal energy storage technologies for buildings: A review, Renewable and Sustainable Energy Reviews, 2012, 16(5): 2394-2433.

[19] Nuytten T, Claessens B, Paredis K, Bael J, Six D, Flexibility of a combined heat and power system with thermal energy storage for district heating, Appl. Energy, 2013, 104: 583-591.

[20] Obara S, Yamada T, Matsumura K, Takahashi S, Kawai M, Rengarajan B, Operational planning of an engine generator using a high pressure working fluid composed of CO_2 hydrate, Appl. Energy, 2011, 88(12): 4733-4741.

[21] Obara S, Okuda M, Shimizu R, Matsumura K, Kawai M, Study of a power generation system for distributed power supplies that utilizes the high-pressure dissociation characteristics and the small difference in the temperature of CO_2 hydrate, Journal of Power and Energy Systems, JSME, 2011, 5(3): 376-387.

[22] Sloan D, Koh A C, Clathrate hydrates of natural gases, CRC Press 2007, New York, USA.

[23] Jerbi S, Delahaye A, Fournaison L, Haberschill P, Characterization of CO_2 hydrate formation and dissociation kinetics in a flow loop, International Journal of Refrigeration 2010, 33: 1625-1631.

[24] Takahata M, Kashiwaya Y, Ouchi M, Ishii K, Effect of catalyst of iron oxide-carbon on methane hydrate formation under weak stirring condition, Tetsu-to-Hagane, 2006, 92(6): 393-400. (In Japanese)

[25] Homepage of Mitsubishi Heavy Industrial Limited, Technical Review 2011 No.4: The Development of the CO_2 heat pump hot water supply unit for business use, Retrieved from http://www.mhi.co.jp/technology/review/pdf/484/484086.pdf (In Japanese)

[26] Narita K. The research on unused energy of the cold region city and utilization for the district heat and cooling. Ph.D. thesis, 1996, Hokkaido University. (In Japanese)

[27] Homepage of Honda Motor Co., Ltd., Gas engine cogeneration for individual houses, Press Information 2011.5.23, Retrieved from http://www.honda.co.jp/factbook/power/cogene/201105/cogene.pdf (In Japanese)

Captions

Fig. 1 Each system for analysis

Fig. 2 Phase diagram of various types of gas hydrates

Fig. 3 System operation on pressure–temperature diagram

Fig. 4 Testing double-pipe heat exchanger used for formation and dissociation of a hydrate

Fig. 5 Test catalyst for increasing gas hydrate formation speed

Fig. 6 Gas hydrate battery system

Fig. 7 Outline of System B

Fig. 8 Ambient temperature of Kitami (cold region of Japan, November 2012–March 2013)

Fig. 9 Demand for electricity and heat power by individual houses in Kitami

Fig. 10 Analysis flow

Fig. 11 Test results of heat cycle of CO_2 gas hydrate

Fig. 12 Analysis results of power equipment operation for the conventional system

Fig. 13 Analysis results of power equipment operation for System A with hydrate formation space 1 m^3

Fig. 14 Analysis results of power equipment operation for System B with hydrate formation space 1 m^3

Fig. 15 Comparison results of fuel consumption of each system

Fig. 16 Output of each system in a representative day

Fig. 17 Analysis results of relation between heat to power ratio and fuel consumption of each system

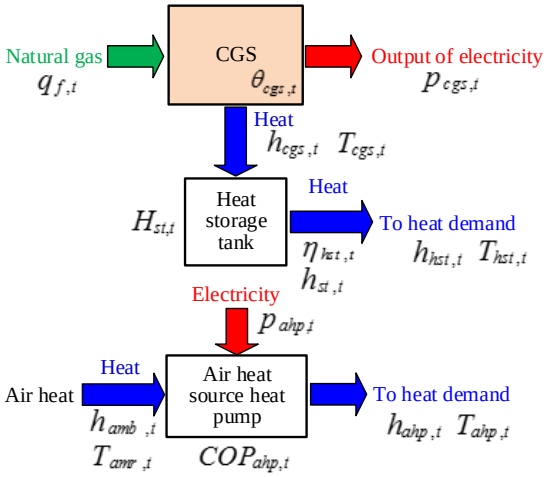

(a) Conventional system

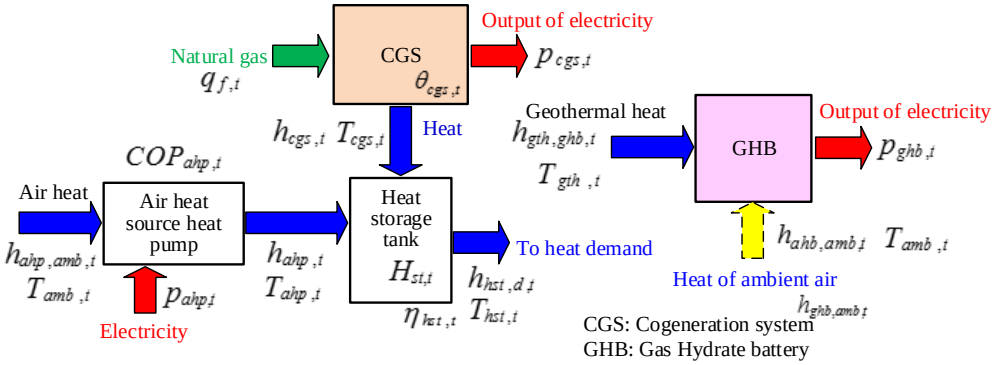

(b) System A

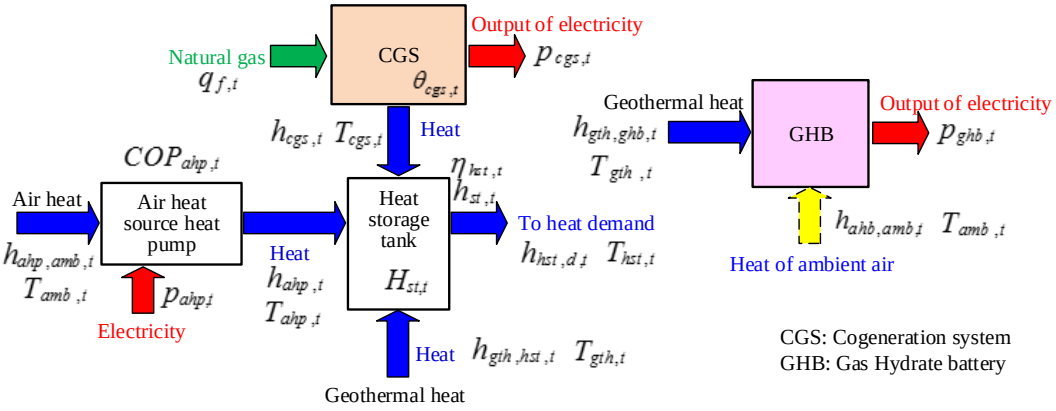

(c) System B

Fig. 1 Each system for analysis

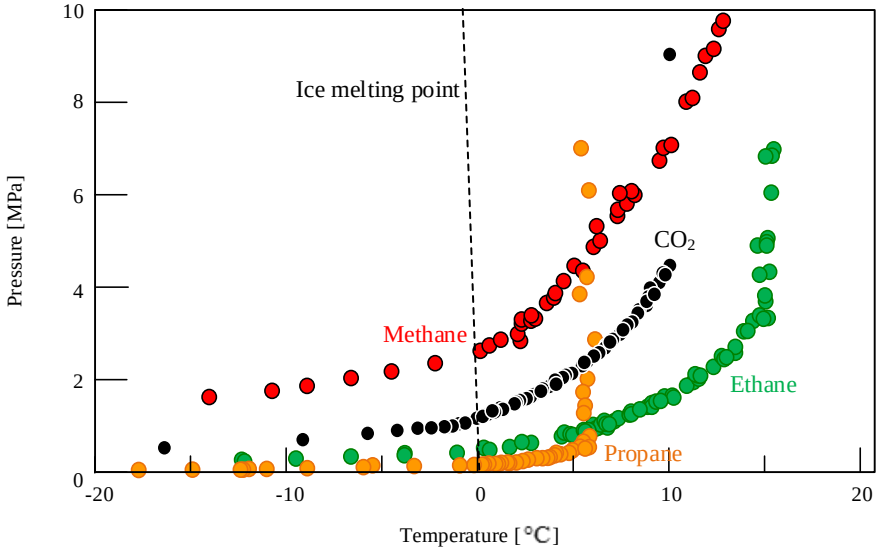

Fig. 2 Phase diagram of various kinds of gas hydrates

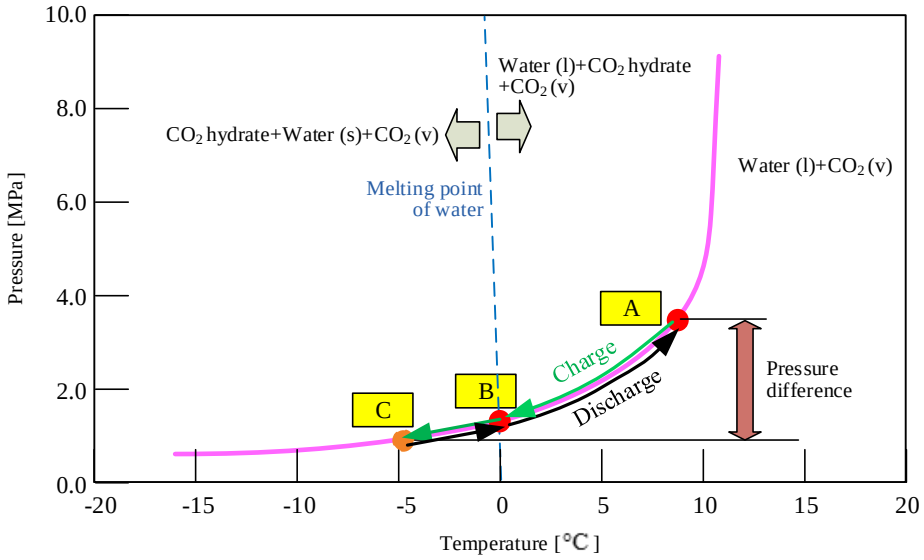

Fig. 3 System operation on pressure-temperature diagram

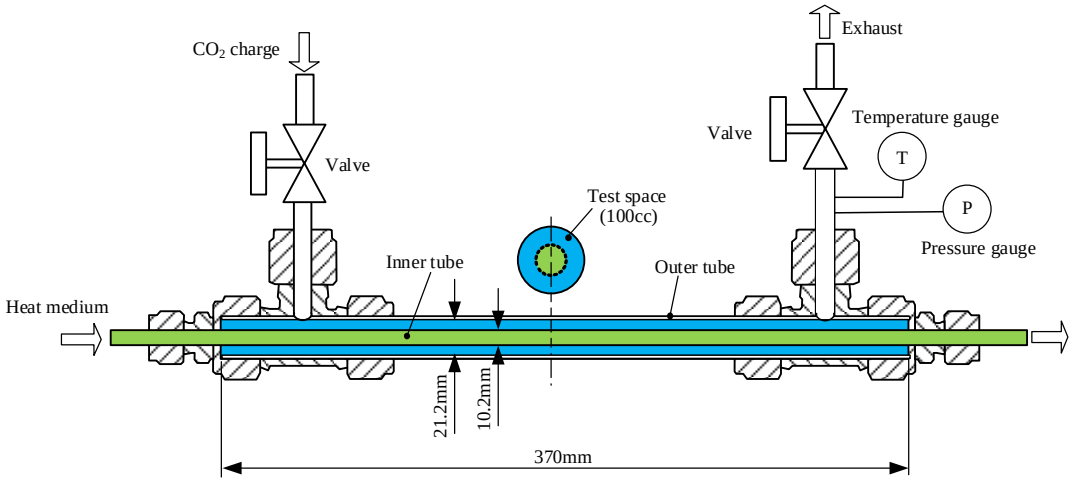

(a) Test heat exchanger

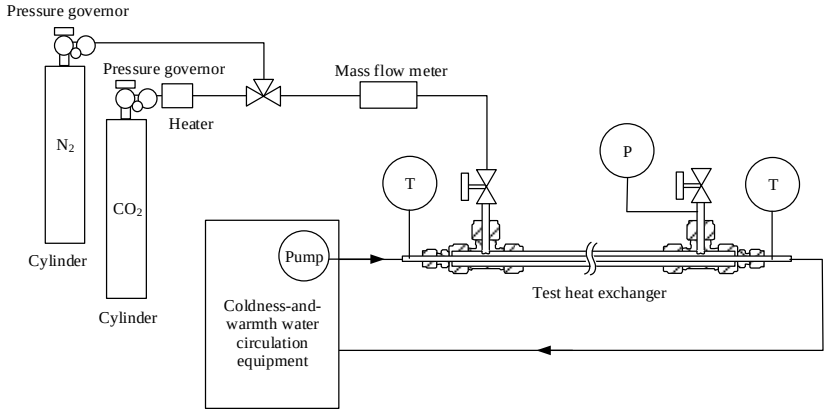

(b) Test equipment

Fig. 4 Testing double-pipe heat exchanger used for formation and dissociation of a hydrate

(a) Before milling processing (b) After milling processing

Fig. 5 Test catalyst for increase of gas-hydrate formation speed

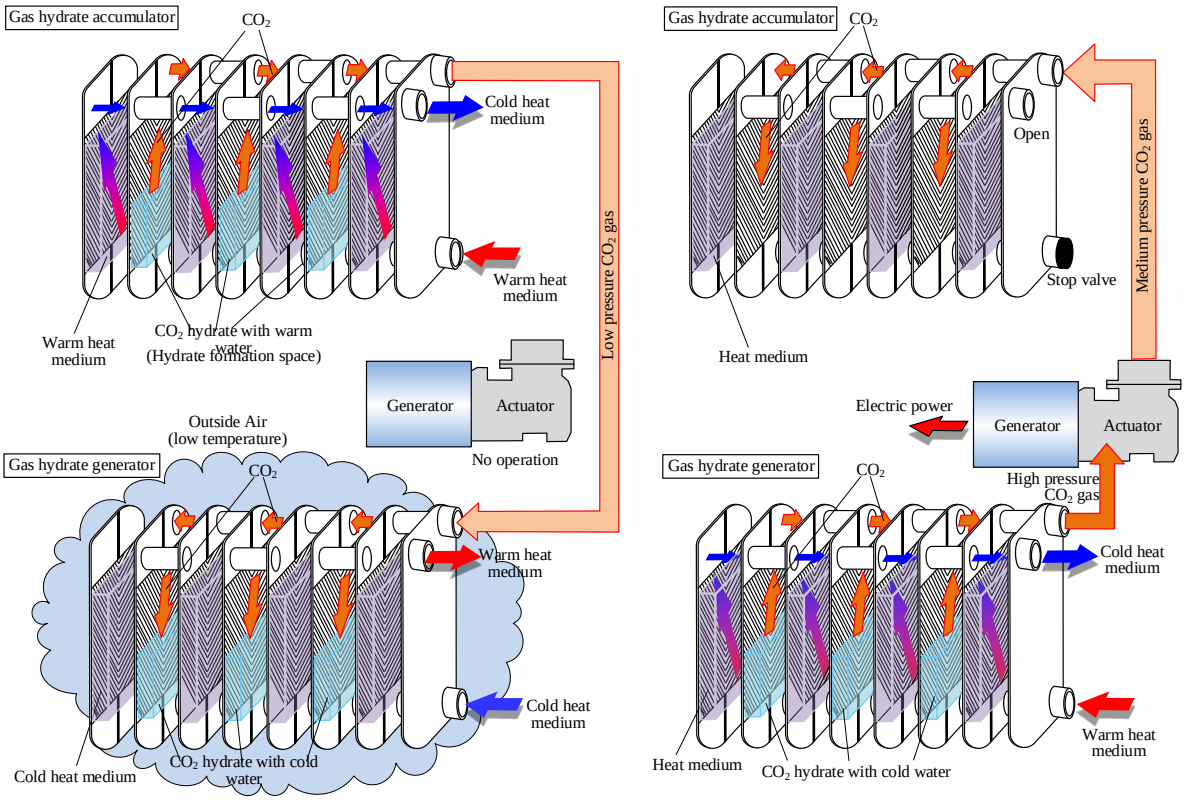

(a) Operation of CO_2 hydrate formation (b) Operation of power generation by dissociation of CO_2 hydrate

Fig. 6 Gas hydrate battery system

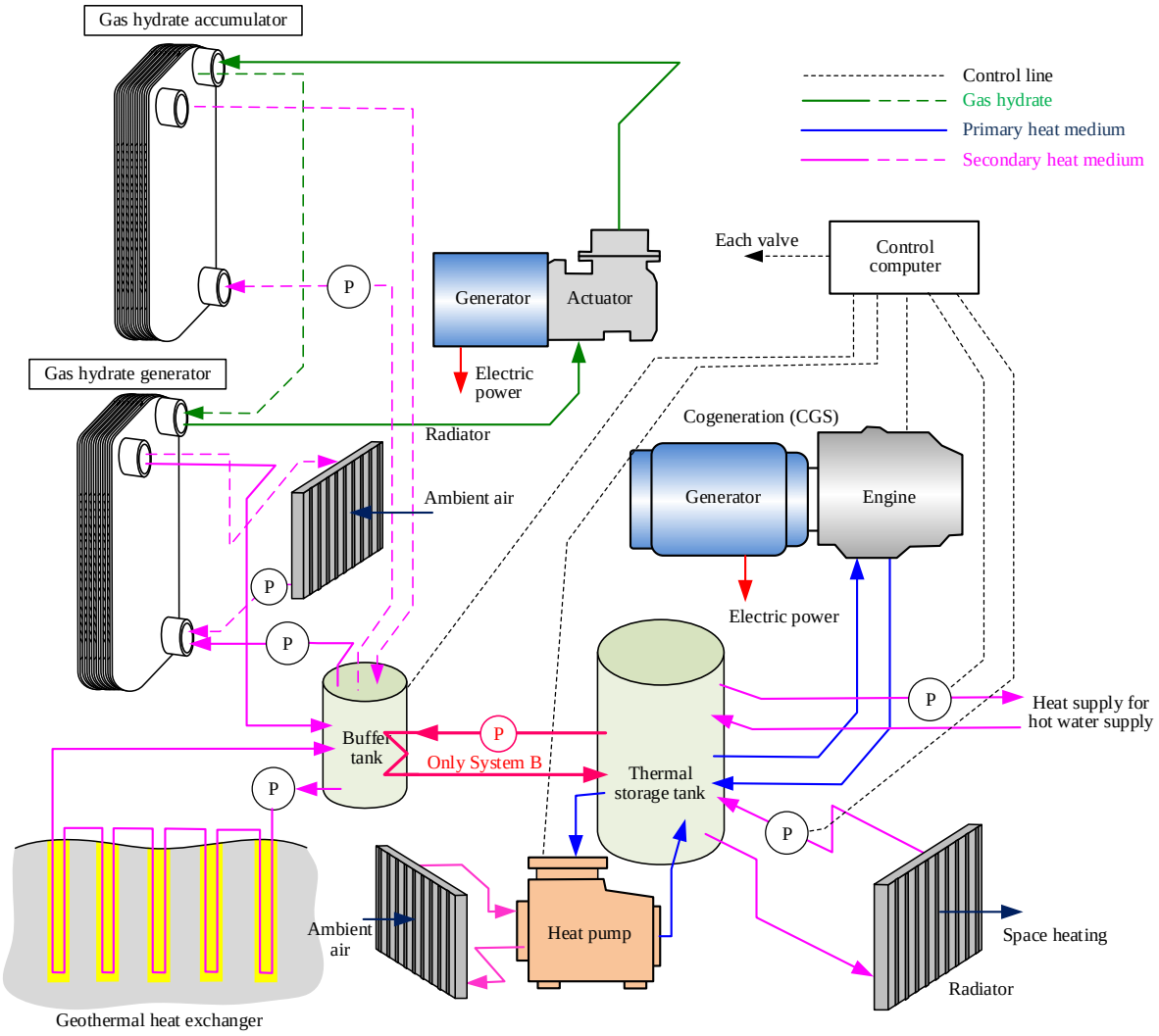

Fig. 7 Outline of System B

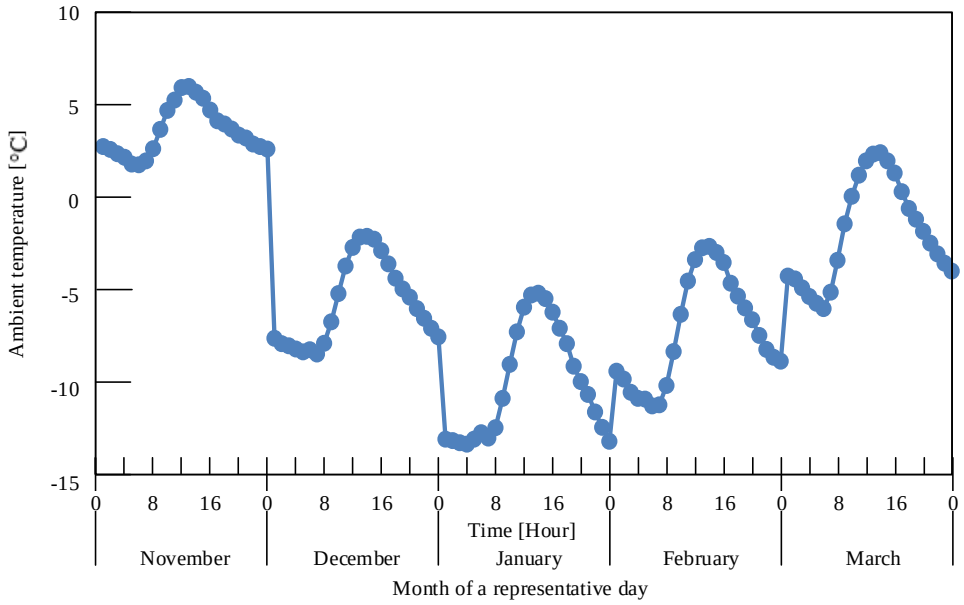

Fig. 8 Ambient temperature of Kitami (November 2012 to March 2013)

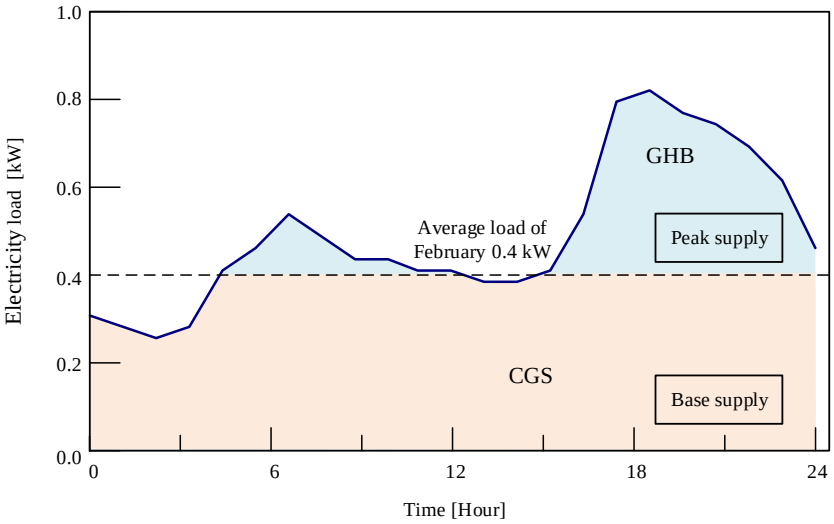

(a) Electricity load of representative day

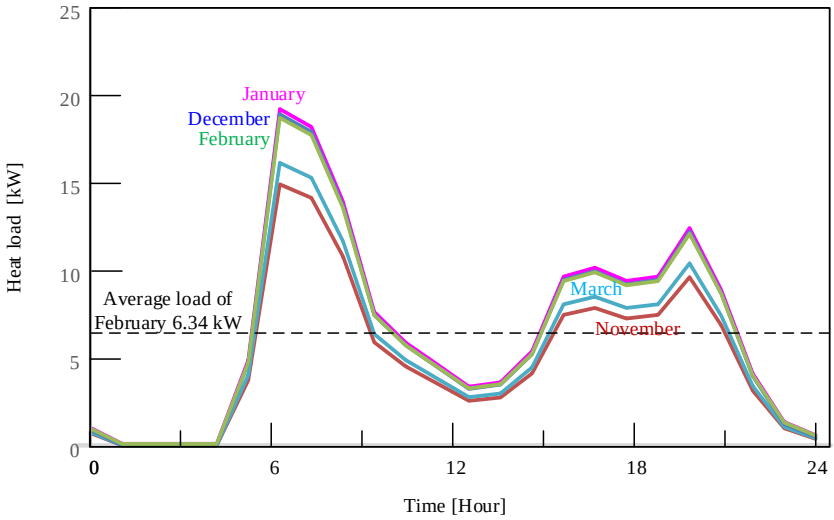

(b) Heat load of representative day

Fig. 9 Demand for electricity and heat power of individual houses in Kitami

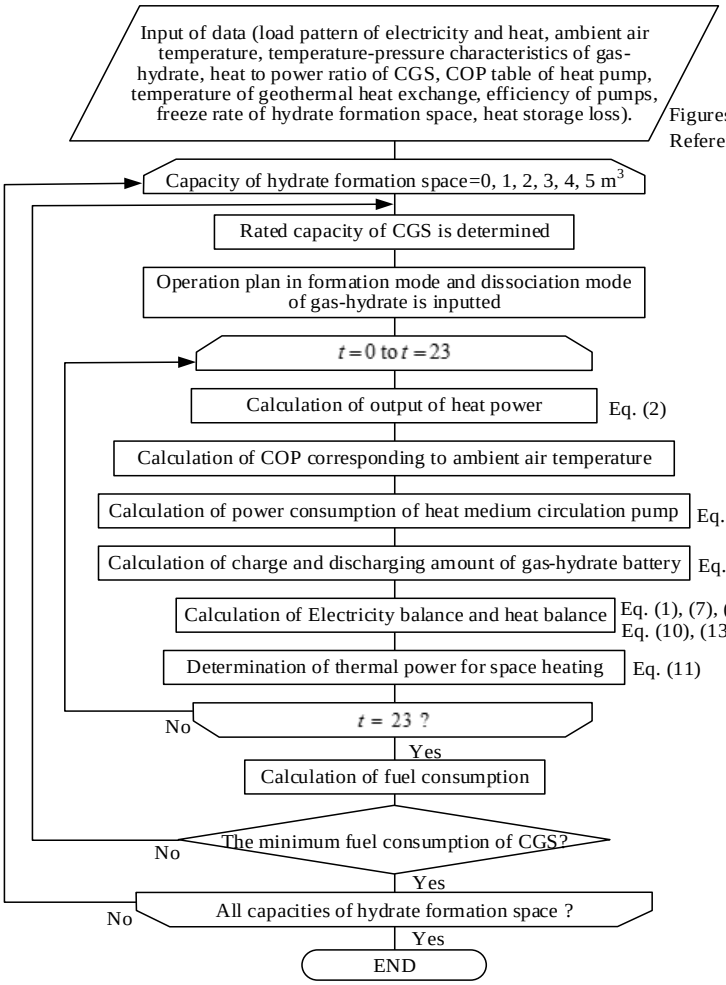

Fig. 10 Analysis flow

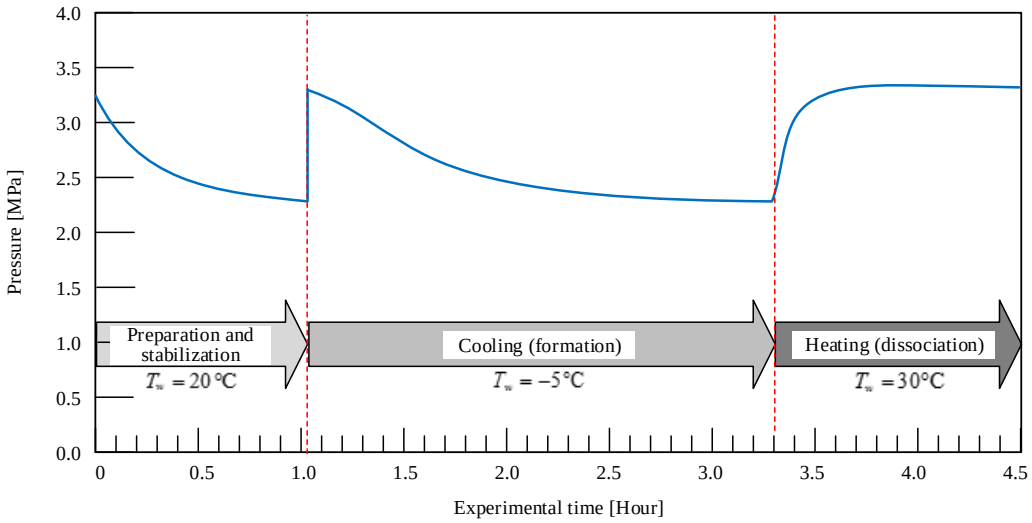

(a) Conventional method

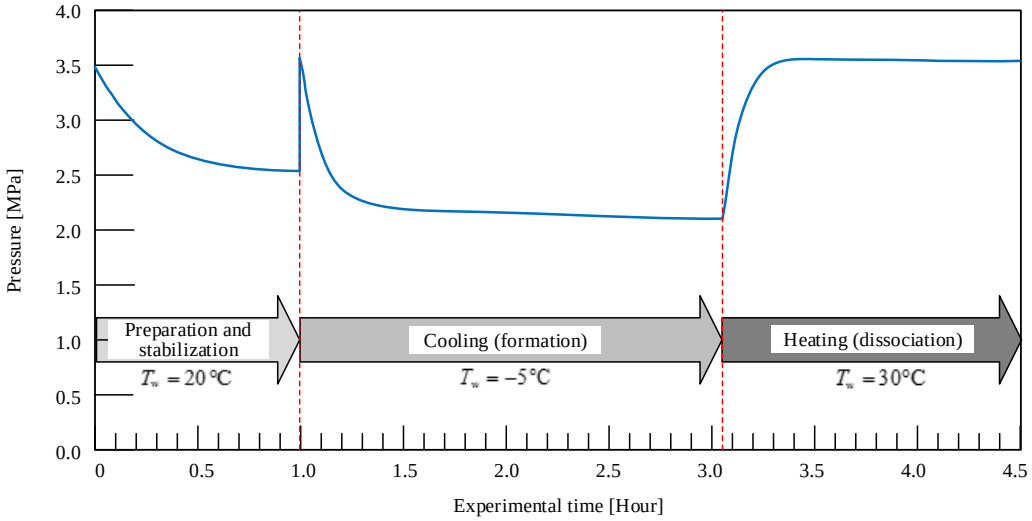

(b) Case using increase catalyst of formation speed

Fig. 11 Test results of heat cycle of CO_2 gas-hydrate

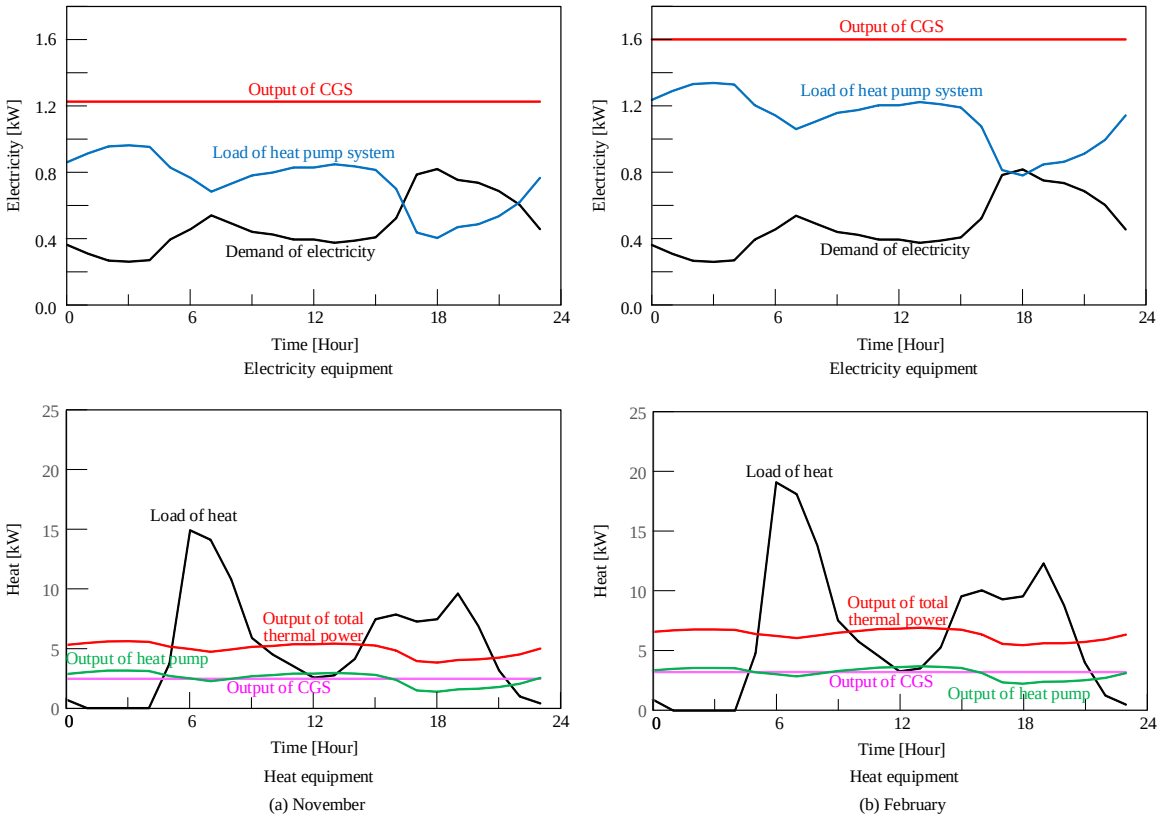

Fig. 12 Analysis results of power equipment operation for the conventional system

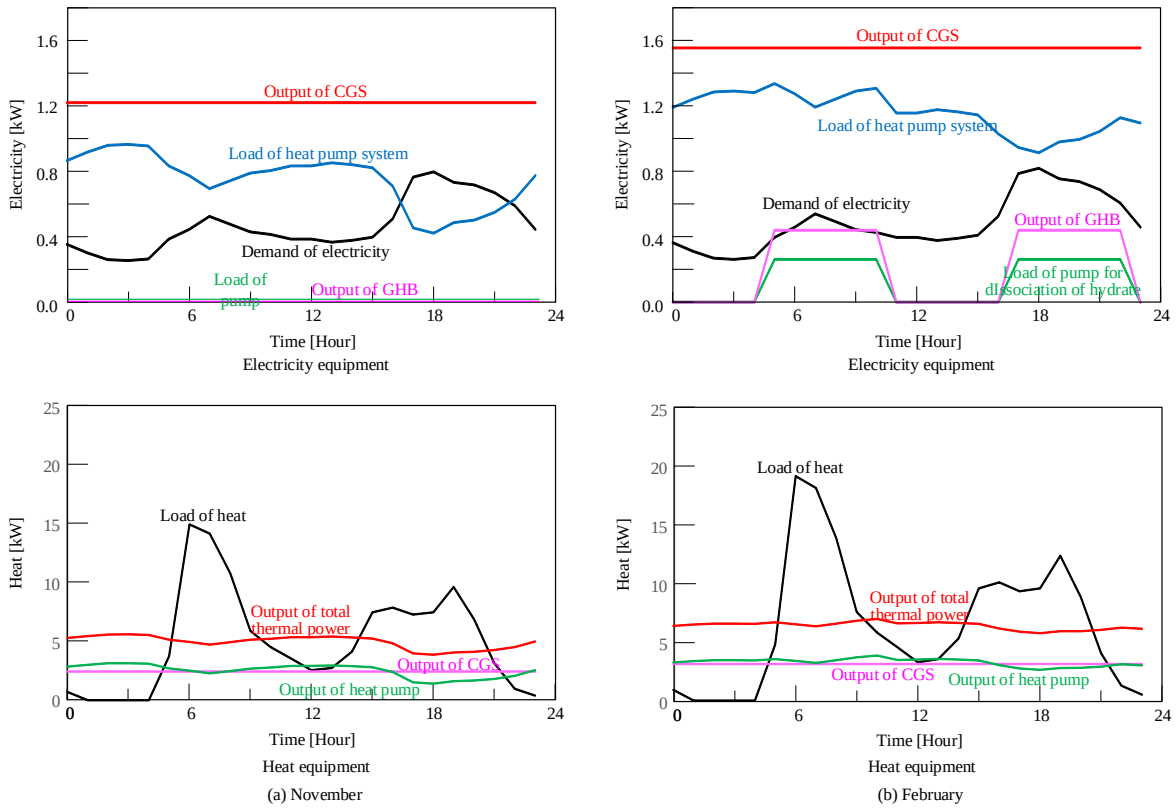

Fig. 13 Analysis results of power equipment operation for System A with hydrate formation space 1m^3

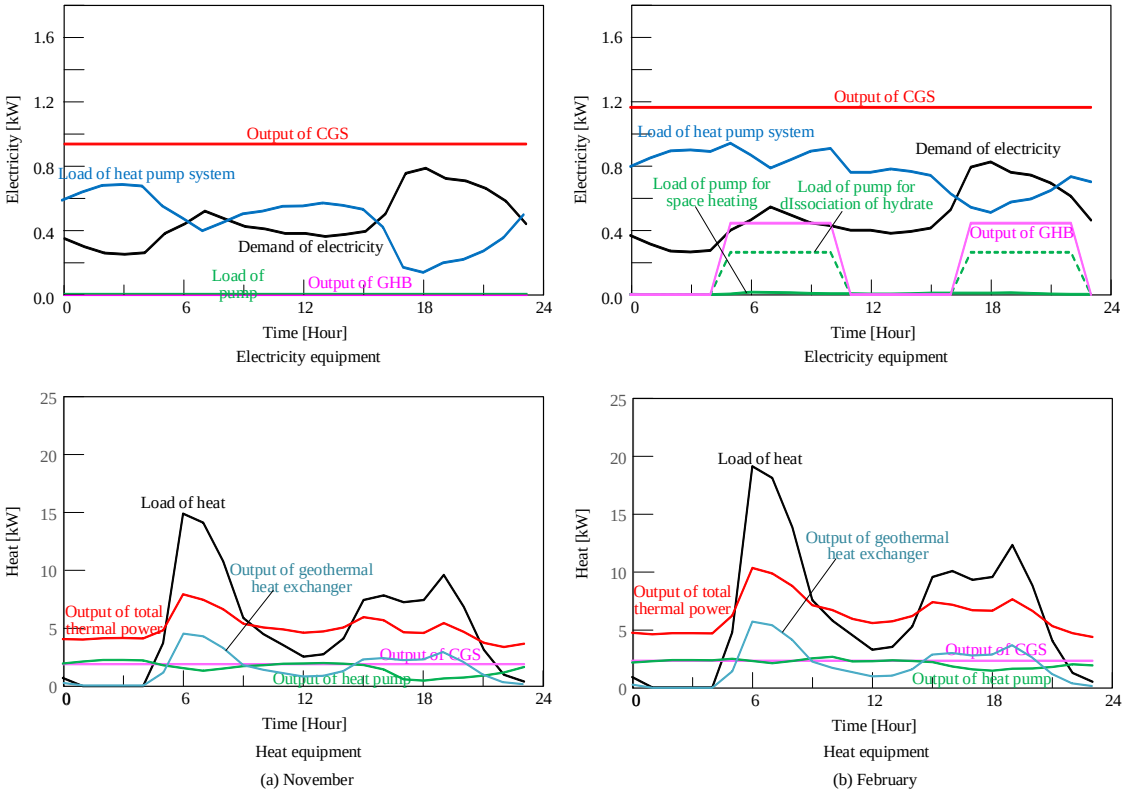

Fig. 14 Analysis results of power equipment operation for System B with hydrate formation space 1m^3

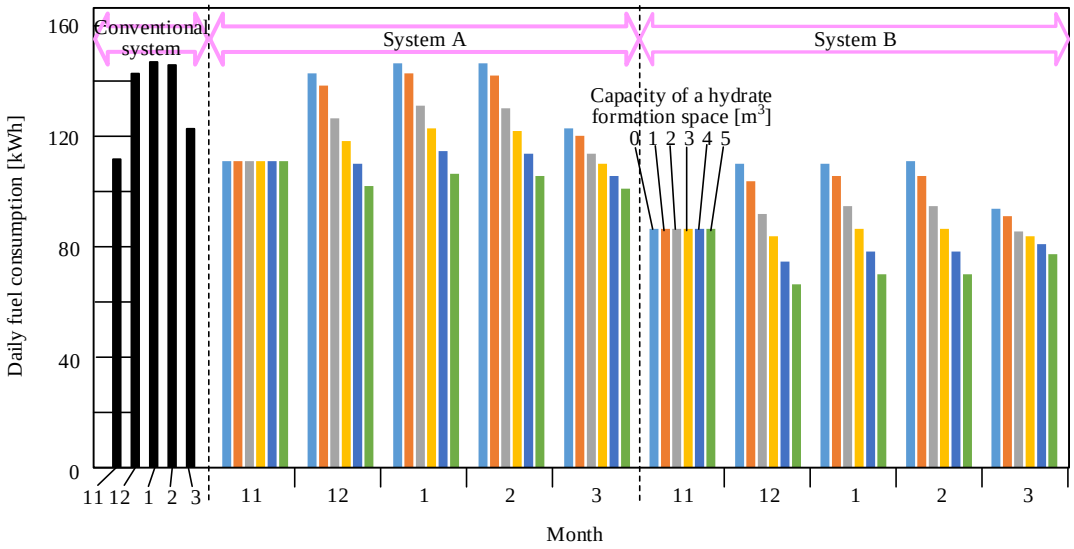

(a) Fuel consumption

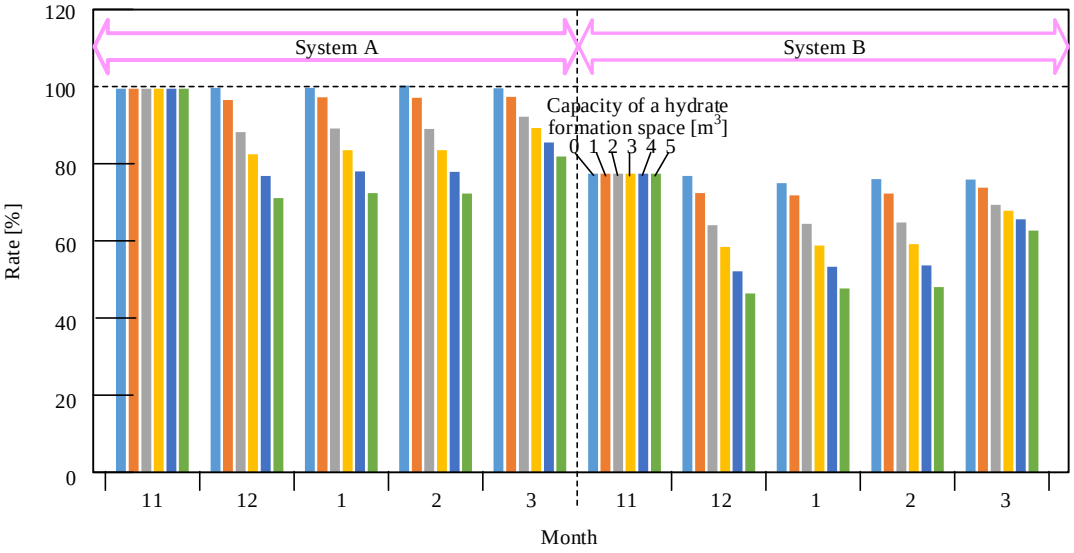

(b) Fuel consumption to the conventional system of each system

Fig. 15 Comparison results of fuel consumption of each system

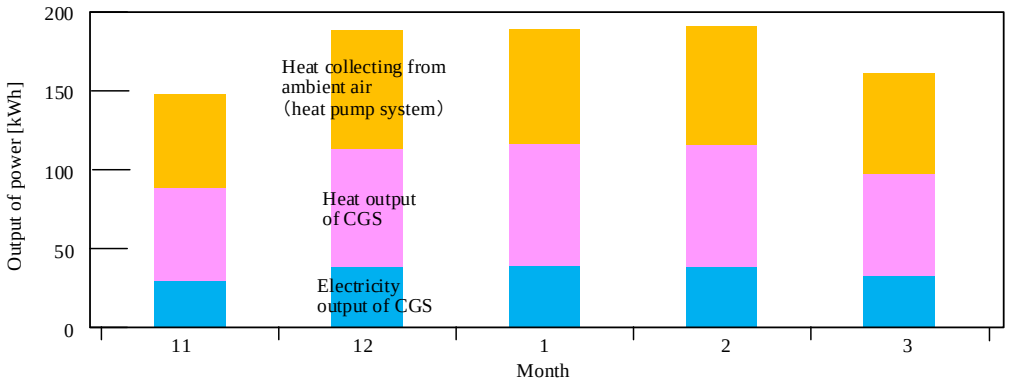

(a) Conventional system

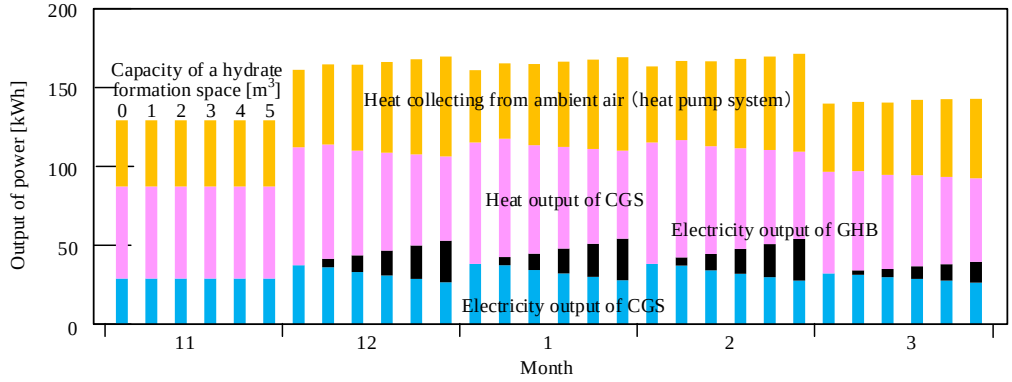

(b) System A

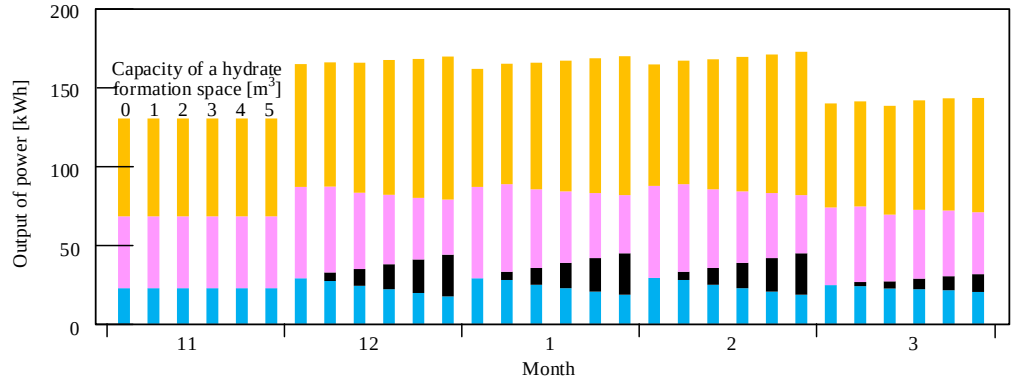

(c) System B

Fig. 16 Output of each system in representative day

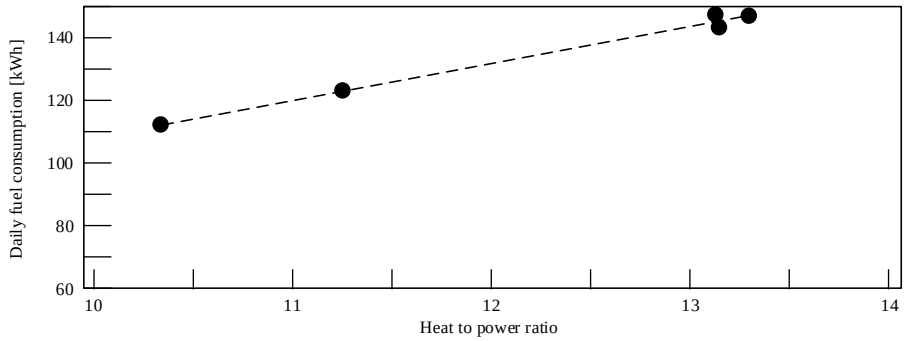

(a) Conventional method

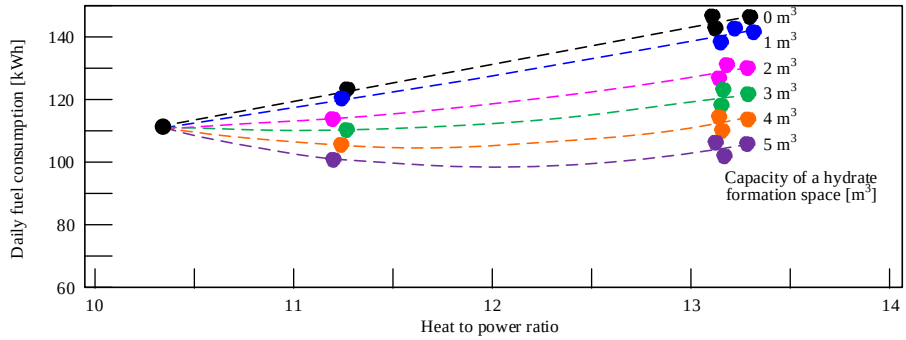

(b) System A

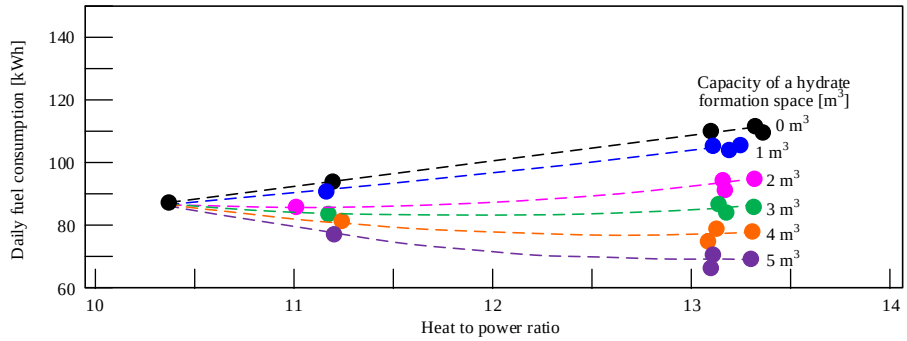

(c) System B

Fig. 17 Analysis results of relation between heat to power ratio and fuel consumption of each system